A Fundamental Equation of State for 1,1,1,3,3-Pentafluoropropane (R-245fa)

Cite as: J. Phys. Chem. Ref. Data **44**, 013104 (2015); https://doi.org/10.1063/1.4913493
Submitted: 22 November 2014 . Accepted: 12 February 2015 . Published Online: 26 March 2015

Ryo Akasaka, Yong Zhou, and Eric W. Lemmon

A Fundamental Equation of State for 1,1,1,3,3-Pentafluoropropane (R-245fa)

Ryo Akasaka
Faculty of Engineering, Department of Mechanical Engineering, Kyushu Sangyo University, 2-3-1 Matsukadai, Higashi-ku, Fukuoka 8138503, Japan

Yong Zhou
Honeywell Integrated Technology (China) Co. Ltd., 430 Li Bing Road, Zhangjiang Hi-Tech Park, Shanghai 201203, People's Republic of China

Eric W. Lemmon
Applied Chemicals and Materials Division, National Institute of Standards and Technology, 325 Broadway, Boulder, Colorado 80305, USA

(Received 22 November 2014; accepted 12 February 2015; published online 26 March 2015)

A new fundamental equation of state explicit in the Helmholtz energy is presented for 1,1,1,3,3-pentafluoropropane (R-245fa), based on recent experimental data for vapor pressures, densities, and sound speeds. The functional form uses Gaussian bell-shaped terms, according to recent trends in the development of accurate equations of state. The independent variables of the equation of state are temperature and density. The equation is valid for temperatures between the triple point (170.0 K) and 440 K, and for pressures up to 200 MPa. Estimated uncertainties in this range are 0.1% for vapor pressures, 0.1% for saturated liquid densities, 0.1% for liquid densities below 70 MPa, 0.2% for densities at higher pressures, 0.3% for vapor densities, 0.3% for liquid sound speeds, and 0.1% for vapor sound speeds. The uncertainties in the critical region are higher for all properties except vapor pressures. The equation shows reasonable extrapolation behavior at extremely low and high temperatures, and at high pressures. [http://dx.doi.org/10.1063/1.4913493]

Key words: equation of state; R-245fa; thermodynamic properties.

CONTENTS

List of Tables

List of Figures

List of Symbols

a	=	molar Helmholtz energy (J mol^{-1})
c_p	=	isobaric heat capacity (J mol^{-1} K^{-1})
c_v	=	isochoric heat capacity (J mol^{-1} K^{-1})
d_i	=	density exponents
e	=	molar internal energy (J mol^{-1})
F	=	relative deviation
h	=	molar enthalpy (J mol^{-1})
l_i	=	density exponents
M	=	molar mass (g mol^{-1})
m_i	=	coefficients
N_i	=	coefficients
n_i	=	coefficients
p	=	pressure (MPa)
p_c	=	critical pressure (MPa)
p_s	=	vapor pressure (MPa)
R	=	universal gas constant (8.314 462 1 J mol^{-1} K^{-1})
s	=	molar entropy (J mol^{-1} K^{-1})
S	=	sum of square of deviations
T	=	temperature (K)
T_c	=	critical temperature (K)
t_i	=	temperature exponents
v	=	molar volume (dm^3 mol^{-1})
W	=	weighting factor
w	=	sound speed (m s^{-1})
Greek symbols		
α	=	dimensionless Helmholtz energy
β_i	=	exponents in the Gaussian bell-shaped terms
γ	=	Gruneisen coefficient
γ_i	=	exponents in the Gaussian bell-shaped terms
δ	=	reduced density ($=\rho/\rho_c$)
ε_i	=	exponents in the Gaussian bell-shaped terms
η_i	=	exponents in the Gaussian bell-shaped terms
ρ	=	density (mol dm^{-3})
τ	=	inverse reduced temperature ($=T_c/T$)
ω	=	acentric factor
Superscripts		
$'$	=	saturated liquid
$''$	=	saturated vapor
0	=	ideal-gas property
r	=	residual property
Subscripts		
0	=	reference state
b	=	normal boiling point
c	=	critical point
calc	=	calculated value
exp	=	experimental value
tp	=	triple point

1. Introduction

1,1,1,3,3-pentafluoropropane (R-245fa) is one of the promising hydrofluorocarbons (HFCs) due to its preferable characteristics as a chemical blowing agent or refrigerant. R-245fa is advantageous over formerly used chlorofluorocarbon (CFC) and hydrochlorofluorocarbon (HCFC) blowing agents in terms of ozone-friendliness and low toxicity characteristics. In the refrigeration industry, R-245fa has been adopted as an alternative for trichlorofluoromethane (R-11) and 2,2-dichloro-1,1,1-trifluoroethane (R-123) in centrifugal chillers and high-temperature heat pumps. In addition, R-245fa has received much attention recently as a working fluid in organic Rankine cycles (ORCs) for the utilization of low-temperature heat sources. There are many experimental or analytical studies for ORCs using R-245fa, e.g., Wei *et al.*,[1] Boretti,[2] Kang,[3] and Luján *et al.*,[4] which concluded that R-245fa is a potential working fluid for ORCs. To improve the thermal efficiency, Agostini *et al.*[5] and Ong and Thome[6] closely investigated boiling heat transfer characteristics of R-245fa. Thermodynamic property information on R-245fa forms the basis of these studies. It is expected that more accurate property information on R-245fa will become available in the future.

A commonly used equation of state for R-245fa is the equation developed by Lemmon and Span[7] in 2006. This equation is a short fundamental equation of state (12 terms) explicit in the Helmholtz energy without Gaussian bell-shaped terms. The equation has suitable accuracies for $p\rho T$ properties in the liquid and vapor phases; however, as shown later, higher uncertainties were found in vapor-pressure calculations. After the Lemmon and Span[7] equation became available, several reliable experimental data sets were published for the vapor pressure and density. The objective of this work is to update the equation for R-245fa based on recent experimental data. This work uses Gaussian bell-shaped terms, according to recent

TABLE 1. Fixed-point properties of R-245fa

Property	Symbol	Value
Molar mass	M	134.047 94 g mol^{-1}
Universal gas constant	R	8.314 462 1 J mol^{-1} K^{-1}
Critical temperature	T_c	427.01 K
Critical pressure	p_c	3.651 MPa
Critical density	ρ_c	3.875 mol dm^{-3}
Triple-point temperature	T_{tp}	170.0 K
Triple-point pressure	p_{tp}	0.011 86 kPa
Saturated liquid density at the triple point	ρ'_{tp}	12.28 mol dm^{-3}
Saturated vapor density at the triple point	ρ''_{tp}	0.839 1 × 10^{-5} mol dm^{-3}
Normal boiling point temperature	T_b	288.198 K
Saturated liquid density at the normal boiling point	ρ'_b	10.18 mol dm^{-3}
Saturated vapor density at the normal boiling point	ρ''_b	0.044 15 mol dm^{-3}
Acentric factor	ω	0.378 3
Reference temperature for ideal-gas properties	T_0	273.15 K
Reference pressure for ideal-gas properties	p_0	0.001 MPa
Reference ideal-gas enthalpy at T_0	${h_0}^0$	54 490.07 J mol^{-1}
Reference ideal-gas entropy at T_0 and p_0	${s_0}^0$	268.219 3 J mol^{-1} K^{-1}

trends in the development of accurate equations of state. These terms allow the equation of state of this work to have better behavior in the critical region. In addition, Gaussian bell-shaped terms can significantly reduce temperature exponents in the polynomial and simple exponential terms. This results in stable behavior of the equation of state at very low temperatures.

The fundamental constants and characteristic properties used in this work are given in Table 1. Other properties are described in Secs. 2–7.

2. Critical and Triple-Point Values

Available experimental data for the critical parameters of R-245fa are given in Table 2. The critical parameters are some of the most important fundamental properties and a prerequisite for the development of an equation of state. They are generally used as the reducing parameters for the independent variables. Since experimental determination of the critical parameters is generally difficult, considerable differences are sometimes observed among reported values. After comprehensive analysis and evaluation, this work adopted the critical temperature and pressure determined by Higashi and Akasaka;[11] their values are (427.01 ± 0.02) K and (3.651 ± 0.003) MPa. The parameters were obtained from direct observation of the meniscus disappearance. The critical temperature was used as the reducing temperature in the new equation of state. It is more difficult to measure the critical density than the other two parameters because of the infinite compressibility at the critical point and the difficulty of reaching thermodynamic equilibrium. Therefore, the critical density determined by Higashi and Akasaka[11] (3.894 mol dm^{-3}) was initially used as the reducing density and was adjusted during the fitting process of the new equation. The final value is 3.875 mol dm^{-3}.

Two experimental values are available for the triple-point temperature. One is 171.05 K reported by Beyerlein *et al.*,[8] and the other is 170.0 K determined by Di Nicola *et al.*[12] This work adopts the value by Di Nicola *et al.*,[12] because the apparatus used in their measurements reproduced triple-point temperatures of several other fluids accurately as compared to reliable literature data. The triple-point pressure and the saturated liquid and vapor densities at the triple point were determined from the new equation of state. The values are given in Table 1 along with the other characteristic values calculated from the new equation of state.

3. Experimental Data

Tables 3 and 4 summarize the available experimental data for R-245fa with the temperatures converted to ITS-90. The tables also give the average absolute deviations (AAD) and bias (BIAS) of each dataset from calculated values with the new equation of state. The AAD and BIAS in any property X are defined as

$$\mathrm{AAD}_X = \frac{1}{N_{\mathrm{exp}}} \sum_{i=1}^{N_{\mathrm{exp}}} |\Delta X_i| \tag{1}$$

and

$$\mathrm{BIAS}_X = \frac{1}{N_{\mathrm{exp}}} \sum_{i=1}^{N_{\mathrm{exp}}} \Delta X_i, \tag{2}$$

TABLE 2. Experimental data for the critical parameters of R-245fa

Author (year)	Critical temperature (K)	Critical pressure (MPa)	Critical density (mol dm^{-3})
Beyerlein *et al.* (1993)[8]	430.65	3.640	3.946
Schmidt *et al.* (1996)[9]	427.20		
Grebenkov *et al.* (2004)[10]	427.158	3.647	3.854
Higashi and Akasaka (2014)[11]	427.01	3.651	3.894

TABLE 3. Experimental data for the saturation properties of R-245fa

Author (year)	Number of data[a]	T (K)	p (MPa)	AAD (%)	BIAS (%)
		Vapor pressures			
Defibaugh and Moldover (1997)[13]	28	252–372	0.019–1.2	0.23	0.23
Sotani and Kubota (1999)[14]	32	293–426	0.13–3.6	0.89	0.72
Bobbo *et al.* (2001)[15]	6	293–313	0.12–0.25	0.11	−0.01
Di Nicola (2001)[16]	51	265–352	0.035–0.76	0.36	−0.36
Bobbo *et al.* (2003)[17]	8	283–343	0.083–0.61	0.41	0.41
Grebenkov *et al.* (2004)[10]	97	242–427	0.0091–3.6	0.66	−0.60
Wang and Duan (2004)[18]	79	255–394	0.022–2.0	0.15	−0.12
Pan *et al.* (2006)[19]	40	253–403	0.019–2.4	0.29	−0.23
Feng *et al.* (2010)[20]	133 (59)	236–427	0.0069–3.7	0.05	0.02
Zhang *et al.* (2013)[21]	12	260–377	0.029–1.4	0.26	−0.18
Maruko *et al.* (2013)[22]	10	310–400	0.23–2.2	0.13	0.06
Higashi and Akasaka (2014)[11]	29 (28)	310–426	0.23–3.6	0.03	−0.00
		Saturated liquid densities			
Beyerlein *et al.* (1993)[8]	6	284–358		0.67	−0.67
Defibaugh and Moldover (1997)[13]	28 (28)	252–372		0.01	0.01
Bobbo *et al.* (2003)[17]	8	283–343		0.09	−0.06
Grebenkov *et al.* (2004)[10]	33	256–427		0.16	−0.14
Maruko *et al.* (2013)[22]	10	310–400		0.06	−0.06
		Saturated vapor densities			
Grebenkov *et al.* (2004)[10]	28 (23)	267–427		2.19	1.48

[a]Numbers given in parentheses indicate the number of data points used in the fit.

where

$$\Delta X = 100\left(\frac{X_{\text{exp}} - X_{\text{calc}}}{X_{\text{exp}}}\right). \quad (3)$$

All experimental data were evaluated in terms of sample purity, experimental uncertainties, and deviations from the Lemmon and Span[7] equation of state. Based on the data evaluation, the most reliable and consistent data were selected for the development of the new equation.

The vapor pressure is the most studied property of all thermodynamic properties of R-245fa. A literature survey found 12 articles containing experimental vapor-pressure data. Figure 1 shows deviations in vapor pressures from the Lemmon and Span[7] equation of state. Lemmon and Span[7] mentioned that in the high-temperature region the vapor pressures by Pan *et al.*[19] and those by Wang and Duan[18] are consistent, but they differ from the data by Grebenkov *et al.*[10] In addition, Feng *et al.*[20] also pointed out that obvious discrepancies are observed among vapor pressures at temperatures near the critical point and below 270 K. Feng *et al.*[20] measured a significant number of vapor pressures over a wide range of temperature with uncertainties of 5 mK for temperature and 0.3 kPa for pressure. The uncertainties are the smallest of all the vapor-pressure data given in Table 3. Above 350 K, the vapor pressures by Feng *et al.*[20] are more consistent with those by Pan *et al.*[19] and by Wang and Duan[18] rather than those by Grebenkov *et al.*[10] The data by Higashi and Akasaka,[11] which are the most recent data, also exhibit very similar trends to the data by Feng *et al.*[20] From these observations, this work selected the vapor pressures by Feng *et al.*[20] below 310 K and those by Higashi and Akasaka[11] above 310 K for fitting the new equation of state. The critical pressure adopted in this work (3.651 MPa) was obtained from extrapolation of the Higashi and Akasaka[11] data.

Although there are only five articles containing experimental data for the saturated liquid density, they are consistent

TABLE 4. Experimental data for the single-phase properties of R-245fa

Author (year)	State	Number of data[a]	T (K)	p (MPa)	AAD (%)	BIAS (%)
			$p\rho T$ data (density)			
Defibaugh and Moldover (1997)[13]	L	1041 (1041)	252–372	0.49–6.5	0.01	0.00
Sotani and Kubota (1999)[14]	L	113	298–343	0.15–200	0.12	0.07
Sotani and Kubota (1999)[14]	V	46	313–343	0.15–0.51	1.10	1.10
Di Nicola (2001)[16]	V	32 (32)	313–367	0.22–0.61	0.20	−0.20
Bobbo *et al.* (2003)[17]	L	200	283–343	0.20–25	0.06	−0.01
Grebenkov *et al.* (2004)[10]	L	121 (121)	256–427	0.030–9.2	0.13	0.01
Grebenkov *et al.* (2004)[10]	V	231 (231)	265–437	0.030–4.3	1.98	1.83
Yin and Wu (2011)[23]	L	114 (114)	294–373	1.0–70	0.03	0.00
			Isobaric heat capacities			
Hwang *et al.* (1992)[24]	L	3	308–323	0.21–0.34	5.00	5.00
			Speeds of sound			
Grebenkov *et al.* (2004)[10]	L	121 (121)	293–353	0.18–7.1	0.08	0.01
Kano and Kayukawa (2013)[25]	V	10 (10)	298–308	0.040–0.18	0.07	−0.07

[a]Numbers given in parentheses indicate the number of data points used in the fit.

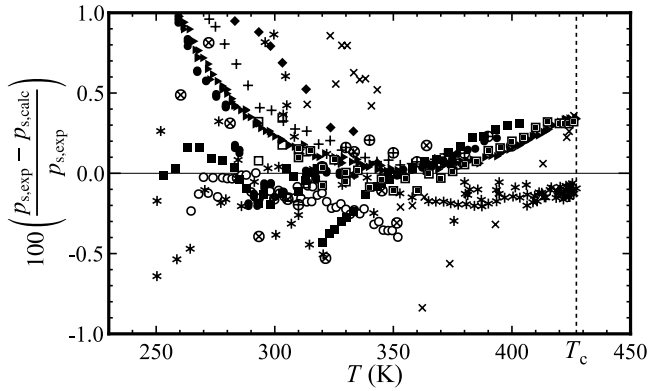

FIG. 1. Percentage deviations between experimental data for vapor pressure and calculated values with the equation of state by Lemmon and Span:[7] (+) Defibaugh and Moldover,[13] (×) Sotani and Kubota,[14] (□) Bobbo *et al.*,[15] (○) Di Nicola,[16] (♦) Bobbo *et al.*,[17] (∗) Grebenkov *et al.*,[10] (•) Wang and Duan,[18] (■) Pan *et al.*,[19] (►) Feng *et al.*,[20] (⊗) Zhang *et al.*,[21] (⊕) Maruko *et al.*,[22] (▣) Higashi and Akasaka.[11]

with each other, except for several data points by Grebenkov *et al.*[10] near the critical point. The data by Beyerlein *et al.*[8] are more scattered than the other data, probably due to lower sample purity and larger uncertainties in the temperature and pressure measurements. The fitting of the equation of state used the data by Defibaugh and Moldover.[13] For the saturated vapor density, only the data by Grebenkov *et al.*[10] are available; the data were used in the fitting process with a small weighting factor.

Six articles report $p\rho T$ data in the single phase. Figure 2 shows the distribution of the $p\rho T$ data. Significant discrepancies are not observed between data points in the liquid phase. At pressures below 10 MPa, the data by Sotani and Kubota[14]

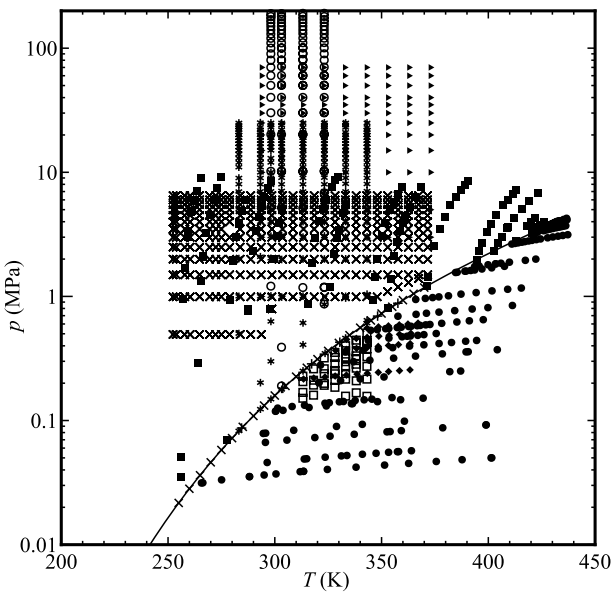

FIG. 2. Distribution of experimental $p\rho T$ data for R-245fa: (+) Beyerlein *et al.*,[8] (×) Defibaugh and Moldover,[13] (□) Sotani and Kubota[14] (vapor), (○) Sotani and Kubota[14] (liquid), (♦) Di Nicola,[16] (∗) Bobbo *et al.*,[17] (•) Grebenkov *et al.*[10] (vapor), (■) Grebenkov *et al.*[10] (liquid), (►) Yin and Wu.[23]

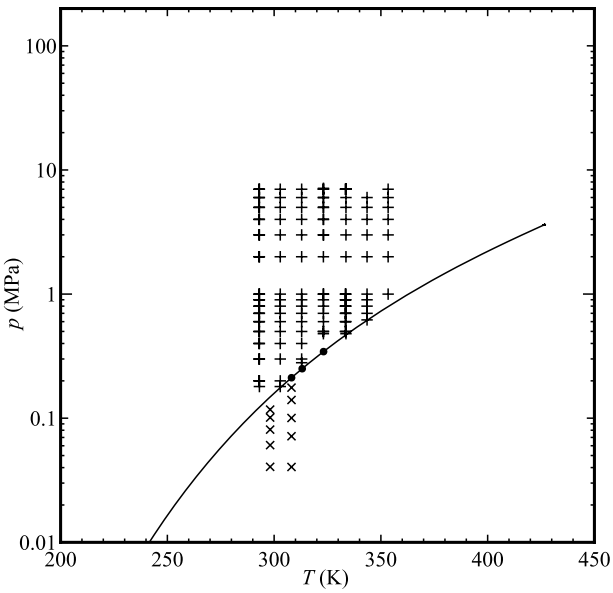

FIG. 3. Distribution of experimental caloric data for R-245fa: (+) Grebenkov *et al.*,[10] (•) Hwang *et al.*,[24] (×) Kano and Kayukawa.[25]

differ slightly from those by Defibaugh and Moldover[13] by about 0.15% in density. On the other hand, the gas-phase data are not consistent with each other. The data by Di Nicola[16] are less scattered than the other data. Although the data by Grebenkov *et al.*[10] cover the critical region, some poor quality data are included. The fitting mainly used the data by Defibaugh and Moldover[13] and by Yin and Wu[23] for the liquid phase and the data by Di Nicola[16] for the vapor phase. The data by Grebenkov *et al.*[10] were also used with very small weighting factors. The liquid-phase data by Sotani and Kubota[14] at 200 MPa were employed to evaluate the equation in the extrapolation region.

There are three articles containing experimental data for the caloric properties. The distribution is shown in Fig. 3. Hwang *et al.*[24] reported isobaric heat capacities at saturation in the liquid phase. Sound-speed data were presented by Grebenkov *et al.*[10] for the liquid phase and by Kano and Kayukawa[25] for the vapor phase. The fitting incorporated sound-speed data with high weighting factors. The heat-capacity data by Hwang *et al.*[24] were not used in the fitting due to larger uncertainties than those in the sound-speed data.

4. Ancillary Equations

For rapid calculation of the saturation properties, simple correlations are presented for the vapor pressure and the saturated liquid and vapor densities. The following correlations were fitted to calculated values obtained with the use of the Maxwell criteria applied to the new equation of state at temperatures from 170 K to the critical temperature. The correlations also provide excellent initial guesses for the iterative calculation required in the Maxwell criteria to determine the saturated state.

The vapor pressure p_s can be represented with the correlation,

$$\ln\left(\frac{p_s}{p_c}\right) = \frac{T_c}{T}\left(N_1\theta + N_2\theta^{1.5} + N_3\theta^{2.5} + N_4\theta^5\right), \quad (4)$$

where T_c is the critical temperature (427.01 K), p_c is the critical pressure (3.651 MPa), $\theta = 1 - T/T_c$, $N_1 = -7.8353$, $N_2 = 1.7746$, $N_3 = -3.1305$, and $N_4 = -3.4216$. The maximum deviation between Eq. (4) and the new equation of state is 0.02% at temperatures between 235 K and 360 K and 0.05% at higher temperatures. Equation (4) represents the selected vapor-pressure data within ±0.1%, except several data points below 250 K.

The correlation for saturated liquid densities ρ' is

$$\frac{\rho'}{\rho_c} = 1 + N_1\theta^{0.17} + N_2\theta^{0.5} + N_3\theta^{1.3} + N_4\theta^{2.5}, \quad (5)$$

where θ is defined as in Eq. (4), ρ_c is the critical density (3.875 mol dm^{-3}), $N_1 = 0.463\ 67$, $N_2 = 2.2375$, $N_3 = -0.275\ 79$, and $N_4 = 0.551\ 36$. Deviations between Eq. (5) and the new equation of state are within ±0.08% at temperatures between 190 K and 425 K. Near the critical point, the maximum deviation is about 0.37%. The selected experimental data for the saturated liquid density are represented by Eq. (5) within ±0.04%.

The saturated vapor densities ρ'' are correlated with

$$\ln\left(\frac{\rho''}{\rho_c}\right) = N_1\theta^{0.24} + N_2\theta^{0.61} + N_3\theta + N_4\theta^{2.7} + N_5\theta^{5.95}, \quad (6)$$

where θ is defined as in Eq. (4), ρ_c is given as in Eq. (5), $N_1 = -0.995\ 83$, $N_2 = -2.6109$, $N_3 = -4.4141$, $N_4 = -18.573$, and $N_5 = -55.961$. Equation (6) reproduces calculated values from the new equation of state within ±0.1% above 230 K, except in the vicinity of the critical point, where the maximum deviation is about 0.3%.

5. Equation of State

The new equation of state is formulated with the Helmholtz energy as the fundamental property with independent variables temperature and density. The form of the equation is

$$\frac{a(T,\rho)}{RT} = \alpha(\tau,\delta) = \alpha^0(\tau,\delta) + \alpha^r(\tau,\delta), \quad (7)$$

where a is the molar Helmholtz energy, α is the dimensionless Helmholtz energy, $R = 8.314\,462\,1$ J mol^{-1} K^{-1} is the universal gas constant,[26] $\tau = T_c/T$ is the inverse reduced temperature, and $\delta = \rho/\rho_c$ is the reduced density. The dimensionless Helmholtz energy α is split into an ideal-gas part α^0 representing ideal-gas properties and a residual part α^r corresponding to the influence of intermolecular forces.

5.1. Ideal-gas Helmholtz energy

The dimensionless ideal-gas Helmholtz energy α^0 is analytically derived from an equation for the isobaric heat capacity of the ideal gas, ${c_p}^0$, as follows:

$$a^0 = h_0^0 + \int_{T_0}^{T} {c_p}^0 dT - RT - T\left[s_0^0 + \int_{T_0}^{T} \frac{{c_p}^0}{T} dT - R\ln\left(\frac{\rho T}{\rho_0 T_0}\right)\right], \quad (8)$$

where $\tau_0 = T_c/T_0$, $\delta_0 = \rho_0/\rho_c = p_0/(RT_0\rho_c)$, T_0 is the temperature at a reference state, p_0 is a reference pressure for the ideal-gas properties, and ρ_0 is the ideal-gas density at (T_0, p_0).

This work used the ${c_p}^0$ equation presented by Lemmon and Span.[7] The equation has the form,

$$\frac{{c_p}^0}{R} = n_0^0 + \sum_{i=1}^{3} n_i^0 \left(\frac{m_i^0}{T}\right)^2 \frac{\exp(m_i^0/T)}{\left[\exp(m_i^0/T) - 1\right]^2}, \quad (9)$$

where the coefficients ${n_i}^0$ and exponents ${m_i}^0$ are given in Table 5. The ideal-gas Helmholtz energy derived from Eqs. (8) and (9) is

$$\alpha^0 = \ln\delta + n_4^0 + n_5^0\tau + \left(n_0^0 - 1\right)\ln\tau + \sum_{i=1}^{3} n_i^0 \ln\left[1 - \exp\left(-m_i^0\tau/T_c\right)\right], \quad (10)$$

where ${n_i}^0$ and ${m_i}^0$ are the same as those in Eq. (9). The values of ${n_4}^0$ and ${n_5}^0$ were determined so that the specific enthalpy and entropy of the saturated liquid state at 0 °C are 200 kJ kg^{-1} and 1 kJ kg^{-1} K^{-1}, respectively, corresponding to the common convention of the refrigeration industry. This results in values of ${h_0}^0$ and ${s_0}^0$ of 54 490.07 J mol^{-1} and 268.2193 J mol^{-1} K^{-1} at the ideal-gas reference state point (T_0 = 273.15 K and p_0 = 0.001 MPa). Table 5 gives additional digits for these coefficients beyond those required to obtain the expected uncertainties to better reproduce the enthalpy and entropy values specified.

5.2. Residual Helmholtz energy

Recent developments of accurate equations of state express the residual Helmholtz energy with the following functional form:

$$\alpha^r(\tau,\delta) = \sum N_i\tau^{t_i}\delta^{d_i} + \sum N_i\tau^{t_i}\delta^{d_i}\exp\left(-\delta^{l_i}\right) + \sum N_i\tau^{t_i}\delta^{d_i}\exp\left[-\eta_i(\delta-\varepsilon_i)^2 - \beta_i(\tau-\gamma_i)^2\right]. \quad (11)$$

In general, the number of terms and the values of the coefficients and exponents are determined through fitting of experimental data. This work fitted the form to the

TABLE 5. Coefficients and exponents of Eq. (9)

i	n_i^0	m_i^0
0	4.0	
1	5.572 8	222 K
2	10.385	1010 K
3	12.554	2450 K
4	−13.385 608 83	
5	9.845 374 371	

TABLE 6. Coefficients and exponents of Eq. (16)

i	N_i	t_i	d_i	l_i	η_i	β_i	γ_i	ε_i
1	0.057 506 623	1.	4					
2	1.561 597 5	0.27	1					
3	−2.361 448 5	0.9	1					
4	−0.517 735 21	1.09	2					
5	0.185 097 88	0.4	3					
6	−0.874 056 26	2.9	1	2				
7	−0.275 309 55	1.7	3	2				
8	0.579 711 51	0.8	2	1				
9	−0.399 343 06	3.6	2	2				
10	−0.033 230 277	1.05	7	1				
11	0.832 105 08	1.8	1		1.011	1.879	1.081	0.709
12	−0.335 443 00	4.	1		1.447	2.454	0.651	0.939
13	−0.101 178 01	4.5	3		1.079	1.256	0.468	0.703
14	−0.009 149 586 7	2.	3		7.86	21.1	1.293	0.777

selected experimental data through the use of the nonlinear fitting algorithm developed by Lemmon and Jacobsen[27] and Lemmon *et al.*[28] The fitting minimized the objective function represented as

$$S = \sum W_\rho F_\rho^2 + \sum W_p F_p^2 + \sum W_w F_w^2 + \cdots, \qquad (12)$$

where W is the weighting factor, and F is the relative deviation in calculated properties from the experimental values. The relative deviations F_p, F_ρ, and F_w are defined as

$$F_p = \frac{p_{\text{exp}} - p_{\text{calc}}}{p_{\text{exp}}}, \qquad (13)$$

$$F_\rho = \frac{p_{\text{exp}} - p_{\text{calc}}}{\rho_{\text{exp}}} \left(\frac{\partial \rho}{\partial p}\right)_T, \qquad (14)$$

and

$$F_w = \frac{w_{\text{exp}} - w_{\text{calc}}}{w_{\text{exp}}}, \qquad (15)$$

where the subscripts calc and exp indicate calculated and experimental values, respectively. The pressure deviation F_p is calculated for $p\rho T$ data in the vapor phase and critical region, and the density deviation F_ρ is calculated for liquid-phase $p\rho T$ data. Deviations for other experimental data were added to the objective function in a similar manner as for the sound-speed deviation F_w.

Each data point is individually weighted according to type, region, and uncertainty. Typical values of W are about 1 for $p\rho T$ data and vapor pressures, 0.01 for heat capacities, and 100 for accurate sound speeds. During minimization of the objective function, various thermodynamic constraints were applied to ensure that the equation of state was well behaved in the vicinity of the critical point and would reliably extrapolate beyond the range of the experimental data. These constraints have been discussed in the literature, e.g., Span and Wagner,[29] Lemmon and Jacobsen,[27] and Lemmon *et al.*[28] For example, the values of the first and second derivatives of pressure with respect to density were fitted so that their values would be zero at the critical temperature and density. The values of t_i should be greater than zero, and d_i and l_i should be integer values greater than zero. Once the minimization finished, the number of significant digits in η_i, β_i, γ_i, and ε_i were rounded to four or less, and those of t_i were reduced to three digits or less, followed by refitting other coefficients and exponents with the same objective function. The final form of the residual part obtained in this work is

$$\alpha^{\text{r}}(\tau,\delta) = \sum_{i=1}^{5} N_i \tau^{t_i} \delta^{d_i} + \sum_{i=6}^{10} N_i \tau^{t_i} \delta^{d_i} \exp\left(-\delta^{l_i}\right) + \sum_{i=11}^{14} N_i \tau^{t_i} \delta^{d_i} \exp\left[-\eta_i(\delta - \varepsilon_i)^2 - \beta_i(\tau - \gamma_i)^2\right], \qquad (16)$$

where the coefficients and exponents are given in Table 6.

6. Comparisons to Experimental Data

Statistical comparisons were made to all available experimental data, including those not used during the fitting. These statistics are based on the AAD and BIAS given by Eqs. (1) and (2). The AAD and BIAS values of the experimental data are given in Tables 3 and 4.

Deviations in experimental vapor pressures from calculated values with the new equation of state are shown in Fig. 4.

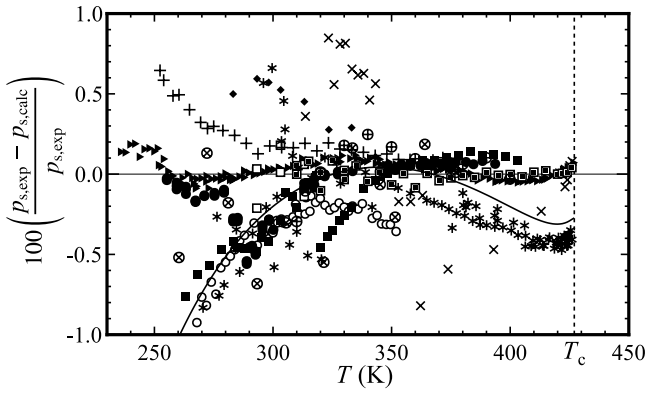

FIG. 4. Percentage deviations between experimental data for vapor pressure and calculated values with the new equation of state: (+) Defibaugh and Moldover,[13] (×) Sotani and Kubota,[14] (□) Bobbo *et al.*,[15] (○) Di Nicola,[16] (♦) Bobbo *et al.*,[17] (∗) Grebenkov *et al.*,[10] (•) Wang and Duan,[18] (■) Pan *et al.*,[19] (►) Feng *et al.*,[20] (⊗) Zhang *et al.*,[21] (⊕) Maruko *et al.*,[22] (⊡) Higashi and Akasaka,[11] (—) Lemmon and Span.[7]

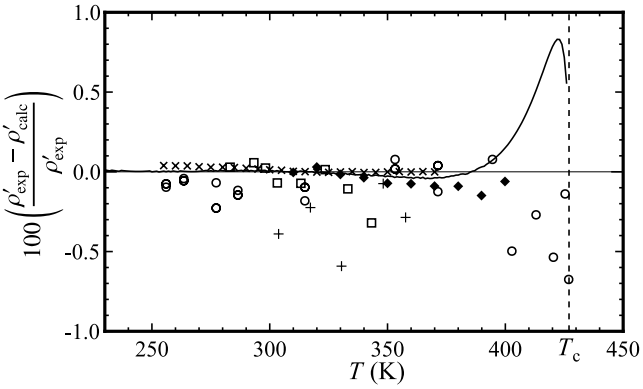

FIG. 5. Percentage deviations between experimental data for saturated liquid density and calculated values with the new equation of state: (+) Beyerlein *et al.*,[8] (×) Defibaugh and Moldover,[13] (□) Bobbo *et al.*,[17] (○) Grebenkov *et al.*,[10] (♦) Maruko *et al.*,[22] (—) Lemmon and Span.[7]

Deviations in calculated values from the equation of state by Lemmon and Span[7] are also plotted in this figure. The data by Feng *et al.*[20] and by Higashi and Akasaka,[11] to which the equation was fitted, are represented within ±0.08%, except some of the data at temperatures below 250 K. The data by Maruko *et al.*[22] are represented within ±0.1% at temperatures above 350 K, but deviate more at lower temperatures, where the maximum deviation is −0.3%. The data by Defibaugh and Moldover[13] show good agreement within ±0.2% at temperatures above 280 K, with increasing deviations at lower temperatures. Although the data by Pan *et al.*[19] show systematic negative deviations down to −0.7% at temperatures below 330 K, the data agree with the equation within ±0.2% at higher temperatures. The data by Di Nicola[16] show systematic negative deviations down to −0.8%. Other vapor-pressure data are represented within ±1%.

Figure 5 shows deviations in the saturated liquid densities from the new equation of state. The data by Defibaugh and Moldover[13] are accurately represented by the equation of state; the largest deviation is 0.039%. The data by Maruko *et al.*,[22] which were not incorporated in the fitting, also show good agreement with the equation of state. Deviations of most of these data are within 0.1%. The data by Grebenkov *et al.*[10] agree with the equation within 0.2% below 400 K, but show larger deviations near the critical point. Systematic negative deviations down to −0.6% are observed in the data by Beyerlein *et al.*[8]

Figure 6 shows deviations in the experimental liquid and vapor densities from the new equation of state. Liquid densities by Defibaugh and Moldover[13] and by Yin and Wu,[23] to which the new equation was fitted, are represented very accurately; their deviations are within ±0.07%. Liquid densities by Bobbo

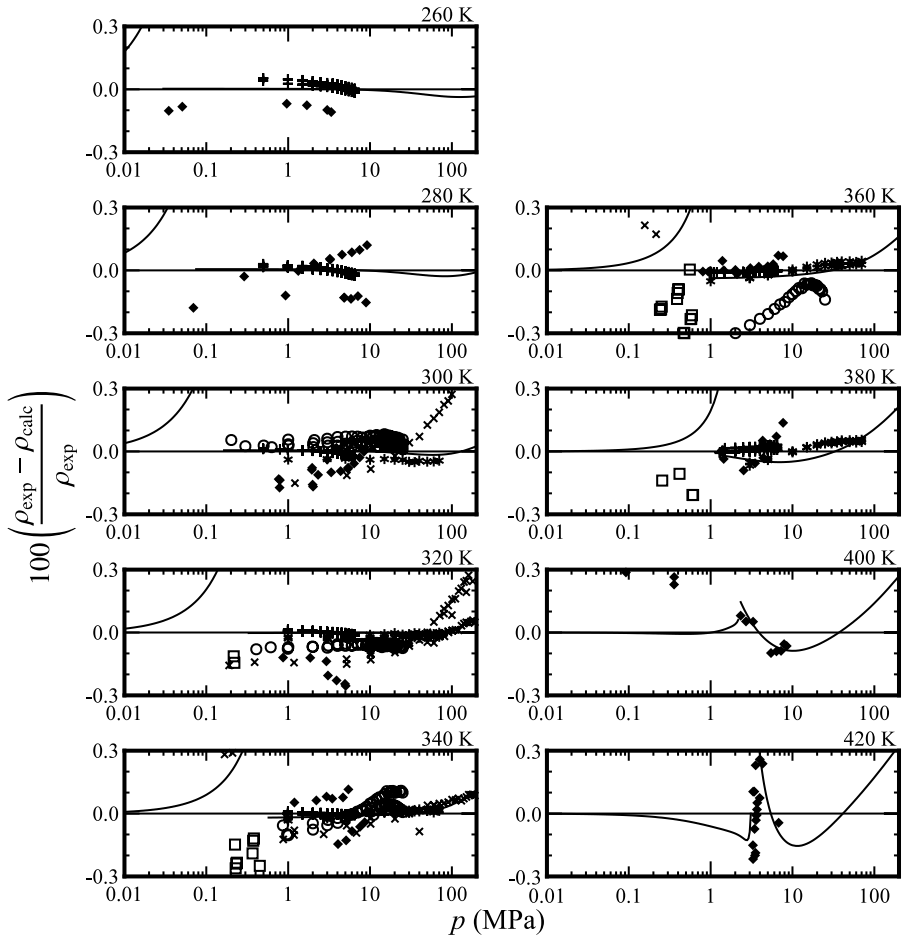

FIG. 6. Percentage deviations between experimental data for density and calculated values with the new equation of state: (+) Defibaugh and Moldover,[13] (×) Sotani and Kubota,[14] (□) Di Nicola,[16] (○) Bobbo *et al.*,[17] (♦) Grebenkov *et al.*,[10] (∗) Yin and Wu,[23] (—) Lemmon and Span.[7]

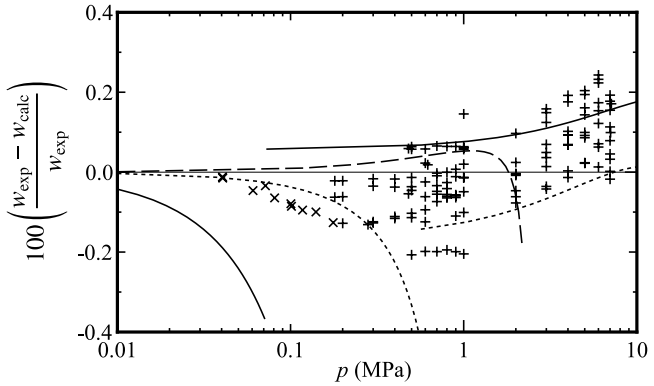

FIG. 7. Percentage deviations between experimental data for sound speed and calculated values with the new equation of state: (+) Grebenkov *et al.*,[10] (×) Kano and Kayukawa.[25] The solid, dotted, and dashed lines indicate deviations from the Lemmon and Span[7] equation at 280 K, 340 K, and 400 K, respectively.

et al.[17] also show good agreement. The data are represented within ±0.1%, except some data at the highest temperatures. Deviations in the liquid densities at 200 MPa by Sotani and Kubota[14] are 0.52% at 298.15 K, 0.34% at 303.15 K, 0.064% at 313.15 K, and 0.10% at 323.15 K. Vapor densities by Di Nicola[16] are reproduced within ±0.36%. The deviation is less than the experimental uncertainty claimed by Di Nicola.[16] Densities by Grebenkov *et al.*[10] are represented by the new equation of state reasonably, except some data near the critical point, where the deviations occasionally exceed 1%.

Deviations in experimental sound speeds from the new equation of state are shown in Fig. 7. At pressures up to 2 MPa, sound speeds in the liquid phase by Grebenkov *et al.*[10] mostly agree with the new equation of state to within ±0.1% but tend to exhibit larger deviations at higher pressures, where the maximum deviation is 0.24%. Sound speeds in the vapor phase by Kano and Kayukawa[25] are represented within ±0.1% except one data point at the highest pressure at 308.15 K.

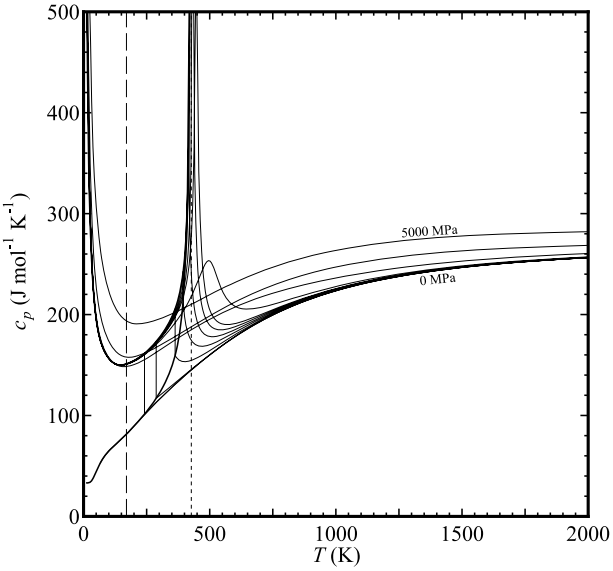

FIG. 9. Isobaric heat capacity c_p versus temperature diagram. Isobars are shown at pressures of 0, 0.01, 0.1, 1, 2, 3, 4, 5, 10, 100, 1000, and 5000 MPa. The dashed line and the dotted line are shown at the triple-point temperature $T_{tp} = 170.0$ K and the critical temperature $T_c = 427.01$ K, respectively.

7. Extrapolation Behavior of the New Equation of State

In order to verify the behavior of the new equation of state in regions away from the available experimental data, several

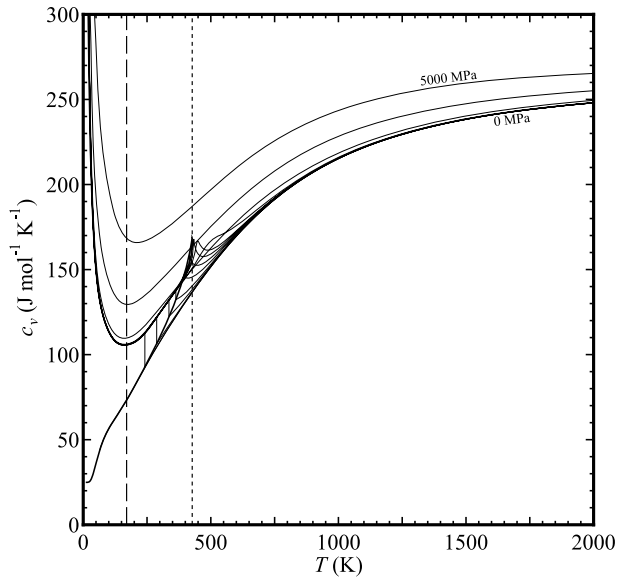

FIG. 8. Isochoric heat capacity c_v versus temperature diagram. Isobars are shown at pressures of 0, 0.01, 0.1, 0.5, 1, 2, 3, 4, 5, 10, 100, 1000, and 5000 MPa. The dashed line and the dotted line are shown at the triple-point temperature $T_{tp} = 170.0$ K and the critical temperature $T_c = 427.01$ K, respectively.

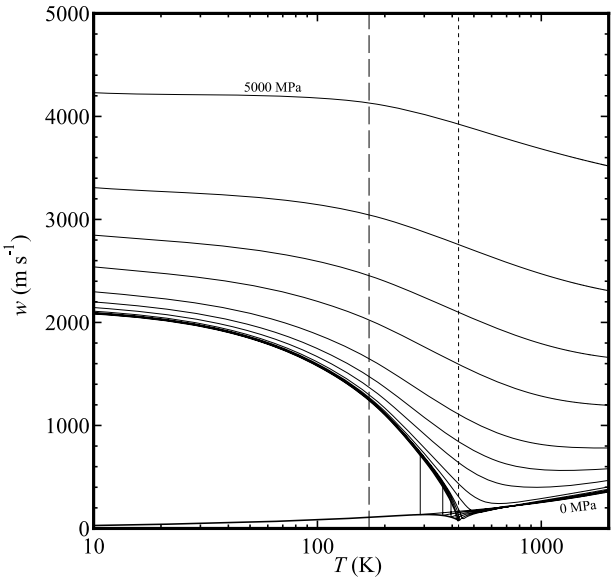

FIG. 10. Sound speed w versus temperature diagram. Isobars are shown at pressures of 0, 0.1, 1, 2, 3, 4, 5, 10, 20, 50, 100, 200, 500, 1000, 2000, and 5000 MPa. The dashed line and the dotted line are shown at the triple-point temperature $T_{tp} = 170.0$ K and the critical temperature $T_c = 427.01$ K, respectively.

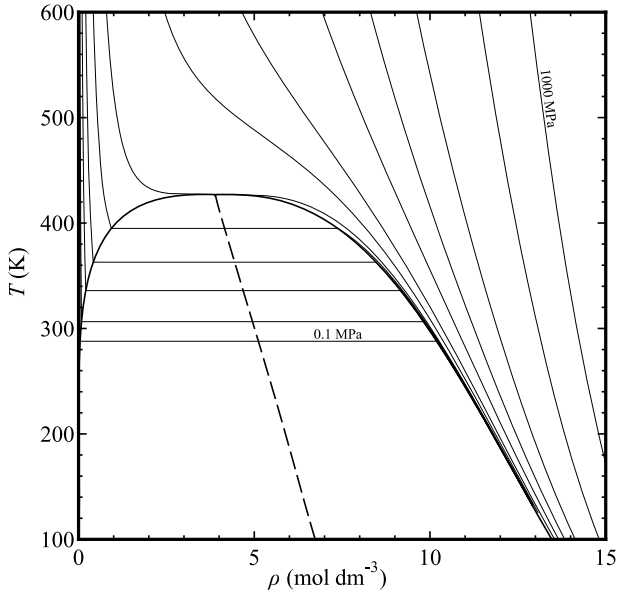

FIG. 11. Isobaric behavior of the equation of state. Isobars are shown at pressures of 0.1, 0.2, 0.5, 1, 2, p_c, 10, 20, 50, 100, 200, 500, and 1000 MPa. The dashed line shows the rectilinear diameter.

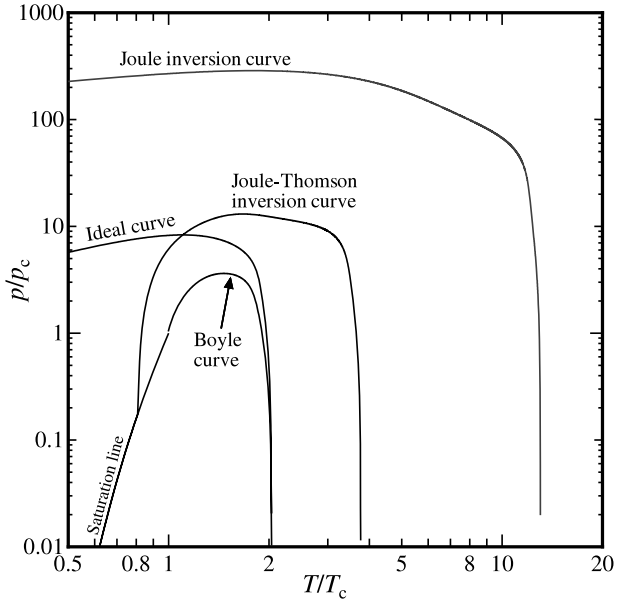

FIG. 13. Characteristic curves of the equation of state as a function of reduced temperature and reduced pressure.

plots of constant-property lines on various thermodynamic coordinates are shown here. Figures 8 and 9 are diagrams for the isochoric heat capacity c_v and isobaric heat capacity c_p versus temperature, respectively. Both figures show that the behavior of the new equation of state is reasonable within the range of validity, and that the extrapolation behavior is also reasonable at higher temperatures and pressures. An upward trend is observed in the liquid region at low temperatures below the triple-point temperature, which is quite common among fluids and has been validated experimentally for many fluids. Figure 10 shows the sound speed w versus temperature. The saturated liquid line on this figure is a smooth arc when displayed on a logarithmic scale. There is no physically incorrect behavior over wide ranges of temperature and pressure.

Figure 11 shows the density behavior along isobars. All isobars are very smooth, and the rectilinear diameter is straight as it approaches the critical point. This helps to ensure that the saturated vapor densities are reliable. Figure 12 indicates that the extrapolation behavior to extremely high temperatures, pressures, and densities is reasonable. As explained by Lemmon and Jacobsen,[27] the smooth behavior at extreme conditions comes from the term with $t_i = 1$ and $d_i = 4$ (the term with the largest d_i in the polynomial terms).

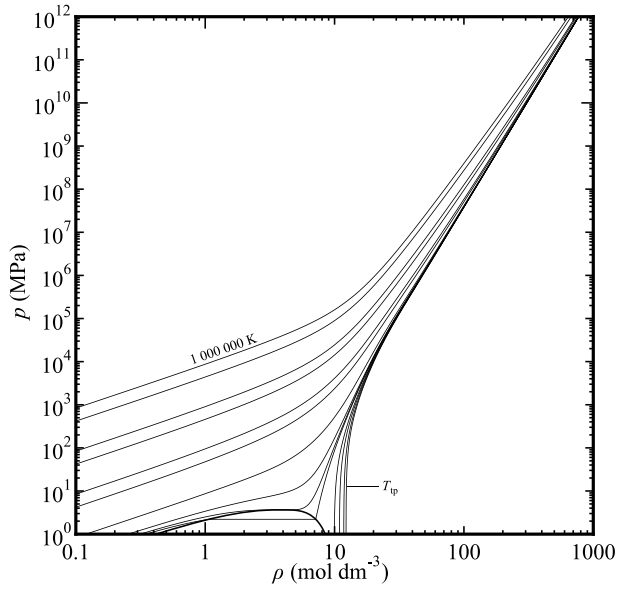

FIG. 12. Isothermal behavior of the equation of state at extreme conditions of temperature and pressure. Isotherms are shown at temperatures of T_{tp}, 200, 250, 300, 400, T_c, 500, 1000, 5000, 10 000, 50 000, 100 000, 500 000, and 1 000 000 K.

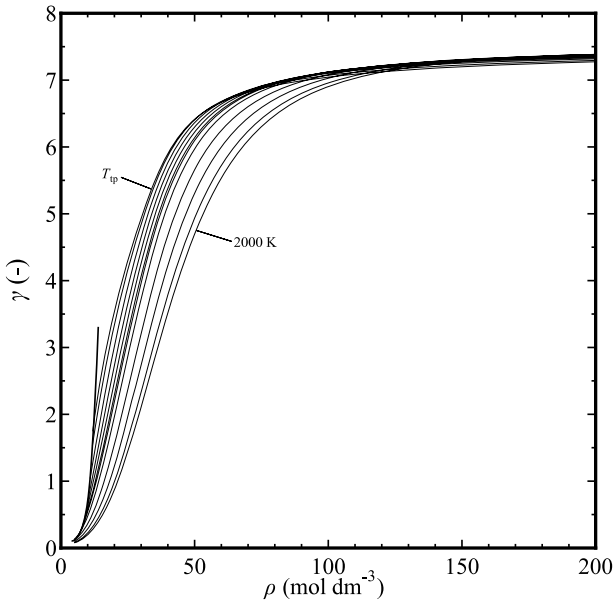

FIG. 14. Gruneisen coefficient γ versus density diagram. Isotherms are shown at temperatures of T_{tp}, 200, 250, 300, 350, 400, T_c, 500, 700, 1000, 1500, and 2000 K.

TABLE 7. Calculated property values from the new equation of state for computer code verification

T (K)	ρ (mol dm^{-3})	p (MPa)	h (kJ mol^{-1})	s (kJ mol^{-1} K^{-1})	c_v (kJ mol^{-1} K^{-1})	c_p (kJ mol^{-1} K^{-1})	w (m s^{-1})
				Saturation state			
250	10.900 57	0.016 460 09	22.9621	0.119 346	0.114 156	0.163 322	873.234
	0.008 011 195	0.016 460 09	51.9442	0.235 275	0.095 083 8	0.103 970	128.702
400	7.151 800	2.210 563	51.5591	0.206 989	0.147 755	0.255 135	235.471
	1.068 455	2.210 563	65.2749	0.241 278	0.148 819	0.234 947	106.449
				Single phase			
250	11	7.454 017	23.3683	0.118 254	0.114 536	0.162 060	908.590
	0.005	0.010 318 29	51.9792	0.239 262	0.094 902 6	0.103 569	129.147
400	9	33.147 25	50.9308	0.196 139	0.144 117	0.188 486	593.178
	0.5	1.352 988	67.9067	0.250 859	0.138 842	0.162 544	135.712

Figure 13 shows the following four characteristic curves: the ideal curve, the Boyle curve, the Joule–Thomson inversion curve, and the Joule inversion curve. Their definitions are given in other work.[28] The behavior of the four characteristic curves is adequate in regions without available experimental data. The Gruneisen coefficient γ is defined as

$$\gamma = v\left(\frac{\partial p}{\partial e}\right)_v, \tag{17}$$

where e is the molar internal energy. Problems with an equation of state can be seen better in plots of the Gruneisen coefficient than with other properties, because the coefficient is a combination of different properties related to the second-order derivatives of the Helmholtz energy. Therefore, the smooth behavior of the Gruneisen coefficient, shown in Fig. 14, suggests that other properties and the equation of state are more likely to be correct.

8. Conclusions

The new equation of state for R-245fa was successfully fitted with the Helmholtz energy as the fundamental property. The new equation is valid for temperatures from the triple point (170.0 K) to 440 K with pressures up to 200 MPa. Comparisons to experimental data demonstrated that typical uncertainties in calculated properties from the new equation are 0.1% for vapor pressures, 0.1% for saturated liquid densities, 0.1% for liquid densities below 70 MPa, 0.2% for densities at higher pressures, 0.3% for vapor densities, 0.3% for liquid sound speeds, and 0.1% for vapor sound speeds. The uncertainties for all properties except vapor pressures increase toward the critical point. In the critical region, the upper value in uncertainty for density is about 1%. Several plots of constant-property lines demonstrated that not only does the new equation exhibit correct behavior over all temperatures and pressures within the range of validity, but also that it shows reasonable extrapolation behavior at higher temperatures and pressures.

As an aid in computer implementation, calculated property values from the new equation of state are given in Table 7.

Acknowledgments

The authors would like to thank the Japan Science and Technology Agency (JST) for a grant that made it possible to complete this study. The authors are also grateful for the suggestions of Eiji Hihara, Shigeru Koyama, Yukihiro Higashi, Akio Miyara, Eiichi Sakaue, Katsuyuki Tanaka, Yohei Kayukawa, Yuya Kano, and Chieko Kondou.

9. References

[1]D. Wei, X. Lu, Z. Lu, and J. Gu, Energy Convers. Manage. **48**, 1113 (2007).
[2]A. Boretti, Appl. Therm. Eng. **36**, 73 (2012).
[3]S. H. Kang, Energy **41**, 514 (2012).
[4]J. M. Luján, J. R. Serrano, V. Dolz, and J. Sánchez, Appl. Therm. Eng. **40**, 248 (2012).
[5]B. Agostini, J. R. Thome, M. Fabbri, B. Michel, D. Calmi, and U. Kloter, Int. J. Heat Mass Trans. **51**, 5415 (2008).
[6]C. L. Ong and J. R. Thome, Exp. Therm. Fluid Sci. **33**, 651 (2009).
[7]E. W. Lemmon and R. Span, J. Chem. Eng. Data **51**, 785 (2006).
[8]A. L. Beyerlein, D. D. DesMarteau, S. H. Hwang, N. D. Smith, and P. A. Joyner, ASHRAE Trans. **99**, 368 (1993).
[9]J. W. Schmidt, E. Carillo-Nava, and M. R. Moldover, Fluid Phase Equilib. **122**, 187 (1996).
[10]A. J. Grebenkov, O. V. Beliayeva, P. M. Klepatski, V. V. Saplitsa, B. D. Timofeyev, V. P. Tsurbelev, and T. A. Zayats, ASHRAE Research Project 1256-RP (2004).
[11]Y. Higashi and R. Akasaka, in *Proceedings of the 7th Asian Conference on Refrigeration and Air Conditioning*, *Jeju, Korea*, *May* (2014).
[12]G. Di Nicola, C. Brandoni, C. Di Nicola, and G. Giuliani, J. Therm. Anal. Calorim. **108**, 627 (2012).
[13]D. R. Defibaugh and M. R. Moldover, J. Chem. Eng. Data **42**, 160 (1997).
[14]T. Sotani and H. Kubota, Fluid Phase Equilib. **161**, 325 (1999).
[15]S. Bobbo, L. Fedele, M. Scattolini, and R. Camporese, Fluid Phase Equilib. **185**, 255 (2001).
[16]G. Di Nicola, J. Chem. Eng. Data **46**, 1619 (2001).
[17]S. Bobbo, L. Fedele, M. Scattolini, and R. Camporese, in *Proceedings of the International Congress of Refrigeration*, *Washington, DC*, *August* (2003).
[18]Z.-W. Wang and Y.-Y. Duan, J. Chem. Eng. Data **49**, 1581 (2004).
[19]J. Pan, J. Wu, and Z. Liu, J. Chem. Eng. Data **51**, 186 (2006).
[20]X. Feng, X. Xu, H. Lin, and Y. Duan, Fluid Phase Equilib. **290**, 127 (2010).
[21]W. Zhang, Z.-Q. Yang, J. Lu, and J. Lu, J. Chem. Eng. Data **58**, 2307 (2013).
[22]K. Maruko, K. Tanaka, and M. Tanaka, in *Proceedings of the 2013 JSRAE Annual Conference*, *Tokyo, Japan*, *September* (2013).
[23]J. Yin and J. Wu, Fluid Phase Equilib. **307**, 1 (2011).
[24]S.-H. Hwang, D. D. DesMarteau, A. L. Beyerlein, N. D. Smith, and P. J. Joyner, Therm. Anal. **38**, 2515 (1992).
[25]Y. Kano and Y. Kayukawa, in *4th IIR Conference on Thermophysical Properties and Transfer Processes of Refrigerants, Delft*, *The Netherlands*, *June* (2013).
[26]P. J. Mohr, B. N. Taylor, and D. B. Newell, Rev. Mod. Phys. **84**, 1527 (2012).
[27]E. W. Lemmon and R. T. Jacobsen, J. Phys. Chem. Ref. Data **34**, 69 (2005).
[28]E. W. Lemmon, M. O. McLinden, and W. Wagner, J. Chem. Eng. Data **54**, 3141 (2009).
[29]R. Span and W. Wagner, Int. J. Thermophys. **18**, 1415 (1997).